Level structure of ^{30}S and its importance in the ^{26}Si(α,p)^{29}P and ^{29}P(p,γ)^{30}S reaction rates

S. Almaraz-Calderon,[*] W. P. Tan, A. Aprahamian, M. Beard, G. P. A. Berg, B. Bucher, M. Couder, J. Görres, S. O'Brien, D. Patel, A. Roberts, K. Sault, and M. Wiescher[†]
Department of Physics, University of Notre Dame, Notre Dame, Indiana 46556, USA

C. R. Brune and T. N. Massey
Department of Physics and Astronomy, Ohio University, Athens, Ohio 45701, USA

K. Fujita, K. Hatanaka, D. Ishiwaka, H. Matsubara, H. Okamura, H. J. Ong, Y. Sakemi, Y. Shimizu,[‡] T. Suzuki, Y. Tameshige,[§] A. Tamii, and J. Zenihiro
Research Center for Nuclear Physics, Osaka University, Ibaraki, Osaka 560-0047, Japan

T. Kubo, Y. Namiki, Y. Ohkuma, Y. Shimbara, S. Suzuki, R. Watanabe, and R. Yamada
Graduate School of Science and Technology, Niigata University, Nishi-ku, Niigata 950-2181, Japan

T. Adachi[‖] and Y. Fujita
Department of Physics, Osaka University, Toyonaka, Osaka 560-0043, Japan

H. Fujita
School of Physics, University of the Witwatersrand, P.O. Wits, Johannesburg 2050, South Africa

M. Dozono and T. Wakasa
Department of Physics, Kyushu University, Fukuoka 812-8581, Japan

(Received 1 April 2012; revised manuscript received 29 October 2012; published 20 December 2012)

The level structure of ^{30}S was studied via the ^{28}Si(^{3}He,n) and ^{32}S(p,t) reactions at the Nuclear Science Laboratory of the University of Notre Dame and the Research Center for Nuclear Physics of the University of Osaka, Japan. Important experimental information on the energy levels, decay branching ratios, and tentative spin assignments is extracted to calculate the reaction rates for ^{29}P(p,γ)^{30}S and ^{26}Si(α,p)^{29}P, which play a critical role in the reaction flow in explosive hydrogen burning.

DOI: 10.1103/PhysRevC.86.065805 PACS number(s): 21.10.Ma, 24.30.−v, 26.30.−k, 26.50.+x

I. INTRODUCTION

The level structure of ^{30}S is key to understanding the αp and the rp processes, as it plays a crucial role in the calculation of the ^{29}P(p,γ) and ^{26}Si(α,p) reaction rates. These two reaction rates are themselves important to understanding explosive hydrogen burning environments like novas and x-ray bursts.

Thermonuclear runaway processes in accreting binary star systems like novas and x-ray bursts are driven by the rp and αp processes along the proton-rich side of the chart of nuclides transferring nuclear material from the hot CNO cycle up to mass $A \sim 40$ [1–3]. For lower temperature environments such as anticipated for Ne novas [4], the reaction flow above $Z = 10$ is driven by the classical rp process, characterized by a sequence of proton capture reactions and β decays transforming material from the Ne, Mg mass region into the Si, S mass region [2,5]. The reaction rates associated with the end point of hydrogen burning in Ne novas are of particular importance for analysis of the abundances in nova ejecta [6].

The ^{29}P(p,γ) reaction rate is therefore of great interest for constraining nova models. The study of presolar grains in the laboratory has been used as a tool for identification of parent stellar sources based on the isotopic signatures [7]. Some of these grains have been identified to be of nova origin [8]. The ^{29}Si and ^{30}Si abundances are good indicators of the peak temperatures achieved in explosions and of the dominant nuclear paths followed in the course of a thermonuclear runaway, leaving a clear imprint on the overall composition of the ejecta [9]. In order to interpret Si abundance measurements, the thermonuclear reaction rates affecting Si production in novas are needed. One of these relevant reaction rates is the ^{29}P(p,γ)^{30}S reaction rate. This reaction rate affects the direct flow away from ^{29}Si (the product of the β^+ decay of ^{29}P) and towards ^{30}Si via the reaction chain ^{29}P(p,γ)^{30}S(β^+)^{30}P(β^+)^{30}Si [10]. A sensitivity study

[*]Present address: Physics Division, Argonne National Laboratory, Argonne, Illinois 60439, USA; salmaraz@nd.edu
[†]mwiesche@nd.edu
[‡]Present address: Center for Nuclear Study, University of Tokyo, Wako, Saitama 351-0198, Japan.
[§]Present address: Office for Development of Proton Therapy Center, Regional Health Services Division, Department of Health and Welfare Fukui Prefectural Government, Fukui City, Fukui Prefecture 910-0846, Japan.
[‖]Present address: Research Center for Electron Photon Science, Tohoku University, Taihaku-ku, Sendai, Miyagi 982-0826, Japan.

performed by Iliadis *et al.* [6] found that ^{29,30}Si abundances changed by about a factor of 3 when the ^{29}P(p,γ)^{30}S reaction was varied within the prescribed limits.

In higher temperature environments such as those anticipated for the atmosphere of accreting neutron stars [1], thermonuclear runaway is driven by the αp process, bypassing the β^+-decay waiting point nuclei of the *rp* process, ^{22}Mg, ^{26}Si, ^{30}S, and ^{34}Ar [3]. The αp process is triggered by the α capture on ^{18}Ne in the hot CNO cycle and proceeds via the reaction sequence ^{18}Ne(α,p)^{21}Na(p,γ)^{22}Mg(α,p)^{25}Al(p,γ)^{26}Si(α,p)^{29}P(p,γ)^{30}S (α,p)^{33}Cl(p,γ)^{34}Ar(α,p)^{37}K(p,γ)^{38}Ca(α,p). Above $Z = 20$ the Coulomb barrier reduces the α-capture reaction rates, which leads to a termination of the αp process. The thermonuclear runaway above $Z = 20$ is predicted to be entirely driven by the *rp* process, as a sequence of proton-capture reactions and β-decay processes. Two of the relevant reaction links are the ^{26}Si(α,p)^{29}P reaction followed by the ^{29}P(p,γ)^{30}S radiative capture process, which take place through resonant states of the compound nucleus ^{30}S, making their reaction rates very sensitive to the level structure of the relevant resonances in ^{30}S. The ^{26}Si(α,p) reaction rate has been identified to play a particularly important role in understanding the observed double-peaked structure in the bolometric luminosity of x-ray bursts. The observed peak separation of 4–7 s [11–13] has been interpreted as a delay in the energy generation and therefore a temporary reduction in the x-ray flux owing to the impedance associated with the ^{26}Si(α,p)^{29}P and ^{34}Ar(α,p)^{33}Cl reactions [14].

The reaction rate predictions for ^{29}P(p,γ) and ^{26}Si(α,p) are uncertain owing to the limited information on the level structure and level characteristics above the proton threshold and the α threshold, respectively. In order to calculate the ^{29}P(p,γ) rate, experimental information on the unbound levels of ^{30}S above the proton threshold at $E_x = 4.399$ MeV up to the α threshold is required. By studying the analog levels in the $A = 30$ isobaric chain, Wiescher and Görres [15], as well as Iliadis *et al.* [16], concluded that the ^{29}P(p,γ) reaction rate at nova temperatures is dominated by two low-lying 3^+ and 2^+ resonances. However, there is no firm experimental evidence for the existence of these 3^+ and 2^+ levels in ^{30}S despite many experimental efforts [17–21]. Using the isobaric-multiplet mass equation, Iliadis *et al.* [16] estimated that the level energies should be $E_x = 4.733$ MeV and $E_x = 4.888$ MeV, respectively. Recent experiments using the ^{32}S(p,t)^{30}S reaction have confirmed a 3^+ energy level at $E_x = 4.699$ MeV [10,22] and showed evidence for the 2^+ resonance level at $E_x = 4.814$ MeV [22]. These results reduced the uncertainties in previous reaction rate predictions considerably, but the resonance strengths used for this calculation still depend on the adopted single-particle spectroscopic factors from the mirror levels in ^{30}Si [22].

The presently adopted rate of the ^{26}Si(α,p) reaction is much more poorly known. No experimental information is available on the level structure of ^{30}S above the α threshold at $E_x = 9.343$ MeV; a high level density was assumed for this excitation range and the presently used reaction rate is based on Hauser-Feshbach predictions. While this assumption has been shown to be valid for the case of the ^{22}Mg(α,p)^{25}Al reaction [23], it still depends on a limited number of natural-parity resonance states which dominate the rate. An independent evaluation of the level density and level parameters in ^{30}S is therefore necessary to confirm the Hauser-Feshbach prediction.

In this work, we studied the resonant level structure of ^{30}S via the ^{32}S(p,t) two-neutron and the ^{28}Si(^{3}He,n) two-proton transfer reactions. The main goal of the first study was to identify proton- and α-unbound levels in ^{30}S and determine the excitation energies with a high accuracy by taking advantage of the high resolving power of the dispersion-matched Grand Raiden (GR) spectrometer at the Research Center for Nuclear Physics (RCNP), Osaka, Japan. The second study aimed at measuring the decay properties of these unbound states by mapping the decay-particle channels in coincidence with the neutrons populating the respective levels. The neutron detector setup at the Nuclear Science Laboratory (NSL) at the University of Notre Dame had only limited time-of-flight (ToF) resolution because of the relatively short flight path but covered a large angle, which improved the overall efficiency.

The combined data from both experiments provide new experimental information on the energies, branching ratios, and tentative spin-parity assignments of several ^{30}S states up to $E_x = 12$ MeV, which are expected to be of great importance in the calculation of the astrophysically important ^{26}Si(α,p)^{29}P and ^{29}P(p,γ)^{30}S reaction rates.

II. THE ^{32}S(p, t) EXPERIMENT

To investigate the proton- and α-unbound states in ^{30}S and to determine the excitation energies with a high accuracy, we performed a ^{32}S(p,t)^{30}S experiment at the Ring Cyclotron facility of the RCNP at Osaka University. This measurement used the same technique as our previous studies of the ^{24}Mg(p,t)^{22}Mg reaction [24] and the ^{28}Si(p,t)^{26}Si reaction [25]. Details of the experimental technique and data analysis are discussed extensively in these works [24,28] and are, therefore, only summarized here.

A 98.7-MeV proton beam from the Ring Cyclotron was transported via the "fully dispersion-matched" WS beam line [29] to the target chamber of the high-resolution GR spectrometer. The proton beam impinged on a 3.38 mg/cm^2, highly enriched ($\geqslant$99%) self-supporting ^{32}S target, sandwiched between two 250 μg/cm^2 Au layers to contain the sulfur under beam bombardment. The target itself was liquid-nitrogen-cooled to allow for beam currents up to 10 nA without loss of target material owing to sublimation. The target thickness translated into an energy spread of roughly 35 keV for the outgoing tritons, which dominated the final resolution at the focal plane of the GR spectrometer [28]. Figure 1 shows a combined ^{30}S spectrum in the full range from the ground state up to 12.3 MeV excitation energy at spectrometer angles of -0.3° and 8.0°. For the identification and subtraction of events from ^{12}C and ^{16}O contaminants, a 1 mg/cm^2 thick ^{12}C target and a 1 mg/cm^2 thick Mylar target were used. The target contamination was low; only the ground state population of ^{14}O was identified below 2 MeV owing to the ^{16}O(p,t)^{14}O background reaction on oxygen contamination trapped between the different target layers. The ground state

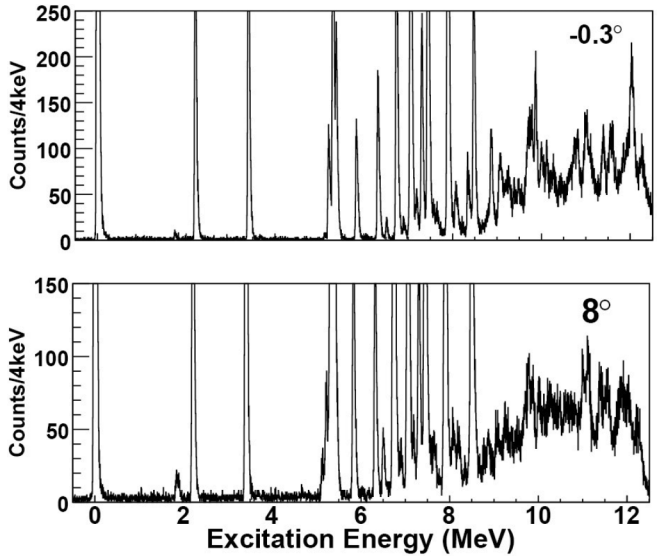

FIG. 1. A combined ^{32}S(p,t)^{30}S spectrum in the range from the ground state up to 12.3-MeV excitation energy is shown for spectrometer angles of -0.3° and 8.0°.

transition of ^{12}C(p,t)^{10}C was identified just below 5.5 MeV and resulted from reactions with ^{12}C surface contamination of the target material. Higher excited states in ^{10}C and ^{14}O contributed only weakly as background to the spectra taken at the high-momentum setting.

The goal of the ^{32}S(p,t)^{30}S experiment was to investigate the nuclear structure of ^{30}S from the ground state up to 12.3-MeV excitation energy. Because of the small momentum acceptance, 5%, of the GR [28] we performed measurements at two different magnetic settings in order to collect spectra over this entire energy with sufficient overlap to obtain a consistent energy calibration. The high-momentum magnetic field of $B_1 = 727.1$ mT covered the excitation range between 0 and 7 MeV, suitable for the study of resonance levels in the ^{29}P(p,γ)^{30}S reaction, while the low-momentum setting of the magnetic field $B_2 = 689.7$ mT covered the excitation range from 6.2 to 12.3 MeV, sufficient for studying the resonance levels in the ^{26}Si(α,p)^{30}S reaction. We took each of these measurements at two angles, -0.3° and 8°, with the purpose of spin-parity identification from the angle-dependent reaction yields.

Calibration of ^{32}S(p,t)^{30}S spectra above the α-emission threshold was done by using the well-known low-lying states as described in Ref. [24]. The absolute calibration of the focal-plane position versus $B\rho$ was performed using the calibration of ^{24}Mg(p,t)^{22}Mg spectra (see Ref. [24]). Therefore, the calculated ^{30}S excitation energies are sensitive to possible uncertainties in the beam energy. Changing the value of the beam energy by 100 keV translates into a change in the ^{30}S excitation energies of up to 0.5 keV for states at a high excitation energy.

Only the uncertainty in the x position in the focal plane is considered a statistical error in the ^{30}S excitation energies. The statistical error is calculated as the FWHM of 35 keV divided by the square root of the number of counts under the peak and is therefore strongly dependent on the statistics. As an example, the statistical error is 3.5 keV for a typical, small peak with 100 counts and 0.78 keV for a large peak with 2000 events. The systematic error includes uncertainties originating from the reaction-angle determination, the mass of ^{30}S (0.5 keV), and the error resulting from the uncertainty in the beam energy (0.5 keV). The uncertainty of 0.5 keV of the mass of ^{30}S is the sum of the uncertainty of 0.3 keV of the mass of ^{30}P [26] and the mass difference of 0.2 keV between ^{30}P and ^{30}S measured by Souin *et al.* [27]. Owing to the method of angular dispersion matching [24] the scattering angle can be reconstructed with an uncertainty of 5 to 8 mrad, depending on the position of the focal plane. This translates into a kinematic error of 0.1 keV at 0° scattering angle and 3.9 and 6.3 keV, respectively, at 8°. These three systematic errors are quadratically added to obtain the total systematic error. The systematic and statistical errors are added linearly to obtain the total error, which is quoted for the present ^{30}S excitation energies. Because of discrepancies between the resulting excitation energies in ^{30}S and the results of previous work [21] a second calibration run was performed using the ^{46}Ti(p,t)^{44}Ti reaction at a 0.92 mg/cm^2, 86.1% isotopically enriched ^{46}Ti target giving consistent results for the energy calibration of the spectra.

III. THE ^{28}Si(^{3}He, n) EXPERIMENT

This experiment was carried out at the NSL at the University of Notre Dame. A 15-MeV ^{3}He pulsed beam with a nanosecond-wide time resolution and 200-ns period was produced by the FN tandem accelerator at the NSL and used to bombard a 90-μg/cm^2-thick self-supported natural Si target provided by Lebow Co. A schematic of the experimental setup is shown in Fig. 2. The reaction products were measured by an array of 16 liquid-organic scintillation detectors which measured the neutrons from the reaction ^{28}Si(^{3}He,n) and a low-energy silicon-strip detector array (LESA) [30,31], which was used to measure the charged particle decays from

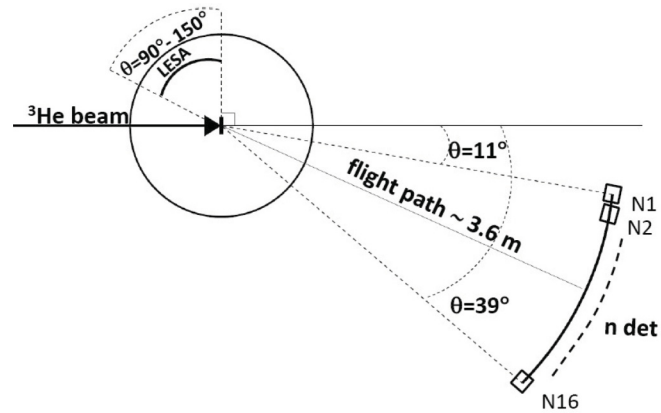

FIG. 2. Schematic of the experimental setup for ^{28}Si(^{3}He,n)^{30}S measurement. The neutron detectors were placed 3.6 m away from the center of the reaction chamber, covering an angular range from 11° to 39°. The silicon detectors (LESA) were placed inside the reaction chamber, covering an angular range from 90° to 150°.

the resonant levels in ^{30}S. The neutron detector array was placed 3.6 m away from the center of the reaction chamber, covering an angular range from 11° to 39°. The beam stop was surrounded by plastic tanks filled with borated water in order to shield the detectors from background neutrons generated at the beam stop. The array of neutron detectors consisted of four hexagonal 12.7-cm (5-in.)-thick detectors, five 17.78 × 2.54-cm (7 × 1-in.) cylindrical detectors, and seven 12.7 × 5.08-cm (5 × 2-in.) cylindrical detectors. The LESA consisted of four identical 300-μm-thick silicon-pad detectors, each of which has four strips 1 cm wide × 4 cm long and a total area of 4 × 4 cm^2. The silicon detector array was installed inside the reaction chamber, 8 cm away from the target center, covering an angular range from 90° to 150°. The neutron and silicon detectors were operated in coincidence mode to measure the decay products of the populated unbound states in ^{30}S.

A measurement with a pure carbon foil was also conducted in order to account for any background from carbon contamination of the target. The environmental background of the neutron ToF spectra was obtained from long runs without beam on target. The energy levels in ^{30}S were identified in the neutron detector array using pulse shape discrimination and ToF methods [32]. The pulse shape discrimination technique was performed with four MPD4 Mesytec modules [33]. The neutron energy obtained from the ToF spectrum was used to identify the populated energy levels in ^{30}S.

A typical neutron ToF spectrum with the identification of different levels in ^{30}S up to $E_x = 10.0$ MeV is shown in Fig. 3. The uncertainties in the ToF spectra are determined by the flight path, the bunching uncertainty, the target thickness, the size of the neutron detectors, and the statistical errors. The systematic and statistical errors are added linearly to account for the total uncertainty in energy. The uncertainties vary with the energy of the neutrons except for the bunching uncertainty, which is a fixed value of 1.5 ns.

Levels above the proton threshold are expected to primarily decay by charged particle emission, with the emitted protons or α's for higher energy states being detected in the LESA.

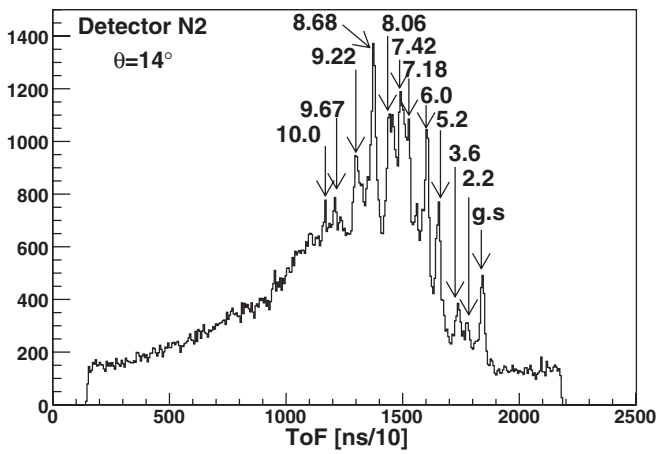

FIG. 3. Neutron ToF spectrum for neutron detector N2 at 14°. Identification of the different levels in ^{30}S up to $E_x = 10$ MeV is shown. Excitation energies in ^{30}S are given in MeV.

A complete kinematics reconstruction was performed to correlate the detected charged particles with the specific neutron group populating the unbound states. The higher energy states in ^{30}S can decay into several proton channels populating excited states in ^{29}P. Primarily observed is proton decay to the ground state of ^{29}P (p channel) and to the first seven excited states in ^{29}P at $E_x = 1.383, 1.954, 2.423, 3.106, 3.448, 4.080$, and 4.343 MeV (channels p^i, p^{ii}, p^{iii}, p^{iv}, p^v, p^{vi}, and p^{vii}, respectively). For α decay primarily transitions to the ground state of ^{26}Si were considered. After identifying the different decay channels, an event-by-event reconstruction for each energy level was made with the specific kinematic shifts for a chosen channel to add up all the 16 strips of the silicon detectors. In the kinematic reconstruction of the proton spectra the resolution is dominated by the intrinsic resolution (∼40 keV) of the silicon detectors and the comparable kinematics energy spread owing to the width of the silicon strips. The energy spread and its effect on the resolution of the kinematics reconstruction are larger at forward angles and smaller at backward angles.

IV. RESULTS AND DISCUSSION

In the data analysis of the ^{32}S(p,t)^{30}S and the ^{28}Si(^{3}He,n)^{30}S experiments, a total of 53 states have been identified in ^{30}S. These states are sorted into three categories, 5 bound states below the proton threshold at 4.4 MeV, 23 proton-unbound states at between 4.4 and 9.34 MeV, and 25 α-unbound states above 9.34 MeV. Of these 53 states, 31 levels have been identified for the first time. In the ^{32}S(p,t)^{30}S experiment, a total of 44 states in ^{30}S have been identified, 25 levels for the first time. A triton spectrum showing the population of the different excited energy levels in ^{30}S is shown in Fig. 1. In comparison, in the ^{28}Si(^{3}He,n) measurement a total of 31 states in ^{30}S were identified; 9 of them were not observed in the ^{32}S(p,t)^{30}S experiment. For the analysis of the ^{28}Si(^{3}He,n) data, the neutron ToF spectra were gated with the signals from the LESA corresponding to charged particle detection, in order to improve the identification of the proton-unbound states in ^{30}S. Typical neutron ToF spectra gated with the LESA signals are shown in Figs. 4 and 5.

In the following we discuss the various bound and unbound levels in ^{30}S based on the analysis of the ^{32}S(p,t)^{30}S and the ^{28}Si(^{3}He,n)^{30}S measurements described above. The spin-parity assignments are guided primarily by the level assignments in the mirror nucleus ^{30}Si. For proton-unbound states large shifts of level energies are expected and the assignments are based on two complementary methods associated with the two experiments. The ^{32}S(p,t)^{30}S reaction was measured for two spectrometer angle settings, −0.3° and 8°. The observed anisotropies in the yields of the various transitions were compared with DWBA predictions for the angular distributions calculated for orbital-momentum transfers of $\ell = 0$, 1, 2, 3, and 4. Higher spin assignments were not considered because previous experiments have indicated that the (p,t) reaction populates preferably low-spin natural parity states [24,25]. Further information is provided by analysis of the proton decay of the populated unbound states in ^{30}S observed in

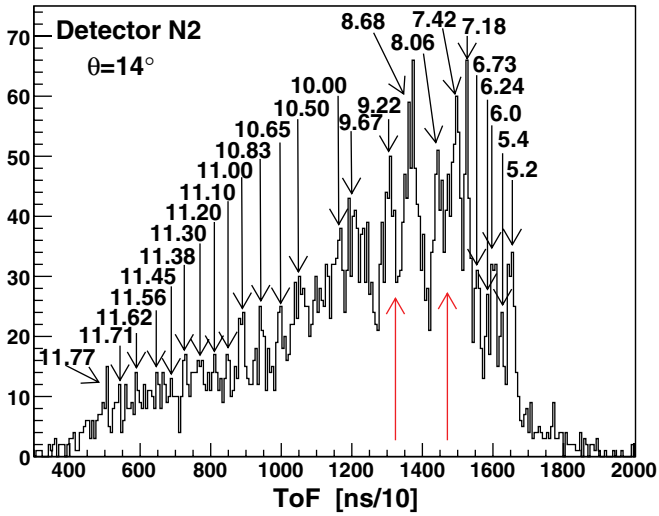

FIG. 4. (Color online) LESA-gated neutron ToF spectrum for neutron detector N2 positioned at 14°. The ^{30}S levels labeled by their excitation energies correspond to those charged particle decays that were measured in the silicon detectors. Arrows indicate the positions of possible background peaks associated with ^{14}O from ^{12}C target contamination. All excitation energies are given in MeV.

the ^{28}Si(^{3}He,n-p$_i$)^{30}S reaction. The strengths of the various proton-decay channels of the populated unbound states were measured using the ^{28}Si(^{3}He,n-p)^{29}P reaction and the energy spectra were reconstructed to extract the proton branching ratios populating different excited states in ^{29}P. These strengths are associated with the orbital-momentum transfers, which provided further limitations for the spin assignments for the unbound states. The reconstructed energy spectra of the decaying particles in coincidence with neutrons are shown in Figs. 6 and 7, with different branching ratios listed in Tables III and V, respectively. The unlabeled peaks in these figures correspond to contamination from neighboring levels.

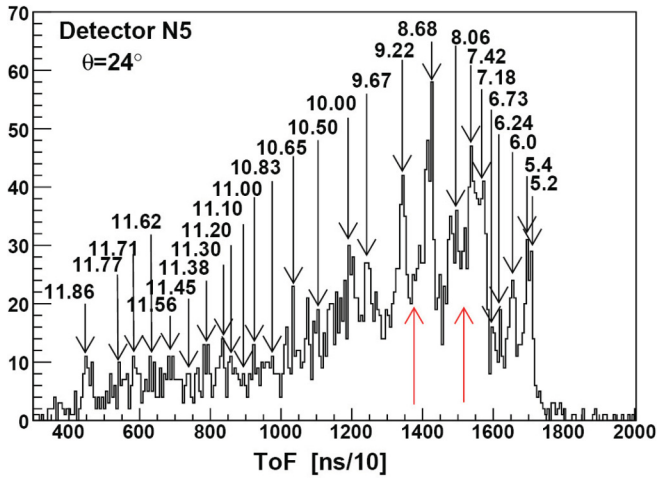

FIG. 5. (Color online) LESA-gated neutron ToF spectrum for neutron detector N5 positioned at 24°. Several unbound levels in ^{30}S are identified with decays recorded by the silicon detectors. Arrows indicate the positions of background peaks of ^{14}O from possible ^{12}C target contamination. All excitation energies are given in MeV.

The decay branching ratios were measured for 15 states in ^{30}S in the ^{28}Si(^{3}He,n-p)^{29}P experiment. Three of these states are above the α-decay threshold.

In the following section the results of the two experiments are discussed for each of the observed levels. Because there is complementary information from both experiments with respect to the specific configuration of the populated states, we first discuss the bound states in ^{30}S in the context of the previously available information. This is followed by a discussion of the level parameters for proton-unbound states, which are of relevance for the determination of the ^{29}P(p,γ)^{30}S reaction. This is followed by a discussion of the observed α-unbound states, which are of relevance for the ^{26}Si(α,p)^{29}P reaction.

A. Bound states in ^{30}S below 4.40 MeV

The bound states in ^{30}S are well known and have been studied by ^{28}Si(^{3}He,n-γ)^{30}S coincidence measurements with a high precision [19]. The excitation energies of the two excited 2^+ states are reported as 2.2107 ± 0.0005 and 3.4026 ± 0.0005 MeV. A doublet was reported at 3.668 ± 0.001 and 3.676 ± 0.003 MeV, corresponding to a doublet in ^{30}Si with 1^+ and 0^+ spin-parity assignments. In the present experiment, the ^{32}Si(p,t) analysis gives excitation energies for the two lowest-lying 2^+ states, at $E_x = 2.2085 \pm 0.0024$ and 3.4058 ± 0.0015 MeV, while the doublet was recorded as an unresolved doublet at 3.6773 ± 0.0071 MeV. The ^{28}Si(^{3}He,n)^{30}S ToF measurements determined excitation energies of $E_x = 2.200 \pm 0.210$ and 3.600 ± 0.260 MeV, with the second 2^+ state and the doublet remaining unresolved owing to the limited resolution associated with the short flight path. These results are in good agreement with recent high-resolution ^{32}S(p,t)^{30}S studies [10,22] except for a small discrepancy in the energy of the second 2^+ state. This agreement demonstrates that the level structure of ^{30}S below the proton threshold is well understood and the level energies serve as additional calibration points for the energy determination of higher-excited states. A summary of the results on the excitation energies of the bound states in ^{30}S in the present ^{32}S(p,t)^{30}S and ^{28}Si(^{3}He,n)^{30}S experiments and a comparison with the results of previous works are reported in Table I.

B. Proton-unbound states in ^{30}S below 9.34 MeV

The analysis of the ^{32}S(p,t) and ^{28}Si(^{3}He,n) transitions to proton-unbound states in ^{30}S agrees well with previous studies. The previous studies were limited to excitation energies below 8 MeV, while the present studies cover considerably higher energies as well. The ^{32}S(p,t)^{30}S spectra indicate 20 proton-unbound levels in this excitation range and the excitation energies could be determined with 10- to 50-keV accuracy, depending on the strength of the various transitions. In comparison, only 12 states were observed in ^{28}Si(^{3}He,n)^{30}S. Despite the rather limited resolution in the ToF measurements, the excitation energy could be reconstructed with improved accuracy by analyzing the proton decays of the various observed levels. A summary of the observed excitation

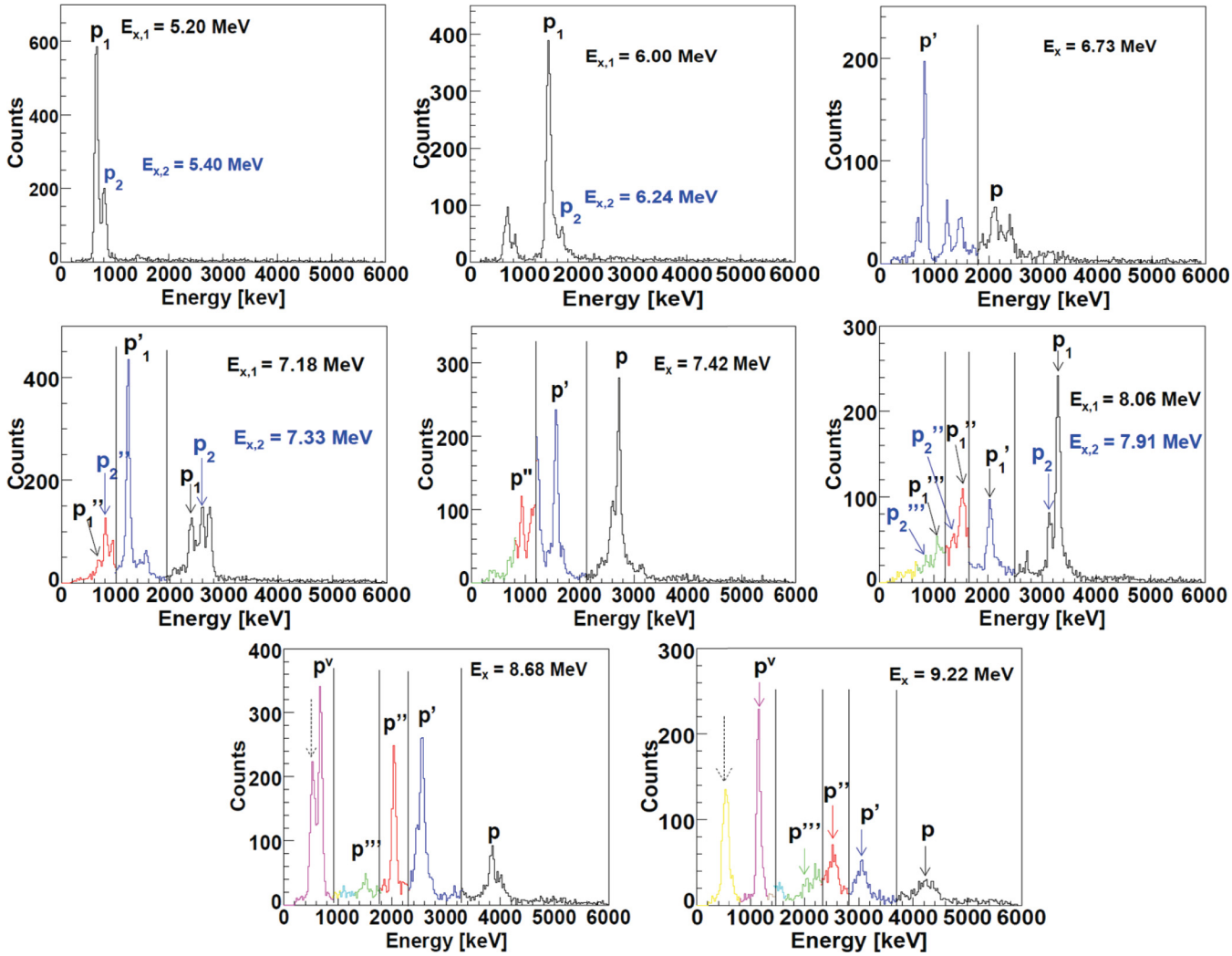

FIG. 6. (Color online) Event-by-event reconstructed spectra for different energy levels in ^{30}S between the proton-decay threshold and the α-decay threshold measured in the present ^{28}Si(^{3}He,n-p) experiment. The different colors separated by vertical lines correspond to the different kinematics used to reconstruct different portions of the spectra. Note that several panels contain peaks corresponding to two different energies as indicated by subscripts, e.g., p_1 belongs to $E_{x,1}$. This is because these peaks are not well resolved in the neutron detectors (ToF spectra) but they are well separated in the LESA, where all the decays are identified and followed. Such is the case for the levels at $E_x = 5.20$ MeV and $E_x = 5.40$ MeV, $E_x = 6.00$ MeV and $E_x = 6.24$ MeV, $E_x = 7.18$ MeV and $E_x = 7.33$ MeV, and $E_x = 8.06$ MeV and $E_x = 7.91$ MeV. In several spectra, contamination from neighboring peaks is observed (unlabeled peaks). The low-energy peak present in the spectra corresponding to $E_x = 8.68$ MeV and $E_x = 9.22$ MeV, marked by the dashed arrow, arises owing to the presence of carbon contamination in the target. Branching ratios are listed in Table III.

energies of the proton-unbound states in ^{30}S up to the α threshold is reported in Table II and compared to the results of previous studies.

The strengths of the various proton-decay channels of the populated unbound states were measured using the ^{28}Si(^{3}He,n-p)^{29}P reaction and the energy spectra were reconstructed to extract the proton-branching ratios populating different excited states in ^{29}P. The reconstructed energy spectra of the decay particles in coincidence with neutrons are shown in Fig. 6, with their corresponding branching ratios listed in Table III. A summary of the states between the proton-decay threshold ($E_x = 4.399$ MeV) and the α-decay threshold ($E_x = 9.343$ MeV) in ^{30}S observed in the ^{28}Si(^{3}He,n-p)^{29}P experiment is also reported in Table III. For these 12 states, information on the excitation energy as well as the branching ratio of the potential resonant levels of ^{30}S is given. These states are relevant in the calculation of the astrophysically important ^{29}P(p,γ)^{30}S reaction rate. In the following we discuss in more detail the experimental observations and the conclusions drawn with respect to the energy and spin-parity assignments of the observed levels.

The first state above the proton threshold at $E_x = 4.6825 \pm 0.0058$ MeV is only weakly observed in the measured ^{32}S(p,t) spectra but corresponds most likely to the previously observed state at 4.704 ± 0.005 MeV [10] and 4.693 ± 0.005 MeV [22]. This level has been identified as the previously predicted low-energy 3^+ state in ^{30}S [10]. The states observed at 5.1300 ± 0.0020 and 5.2178 ± 0.0029 MeV correspond to

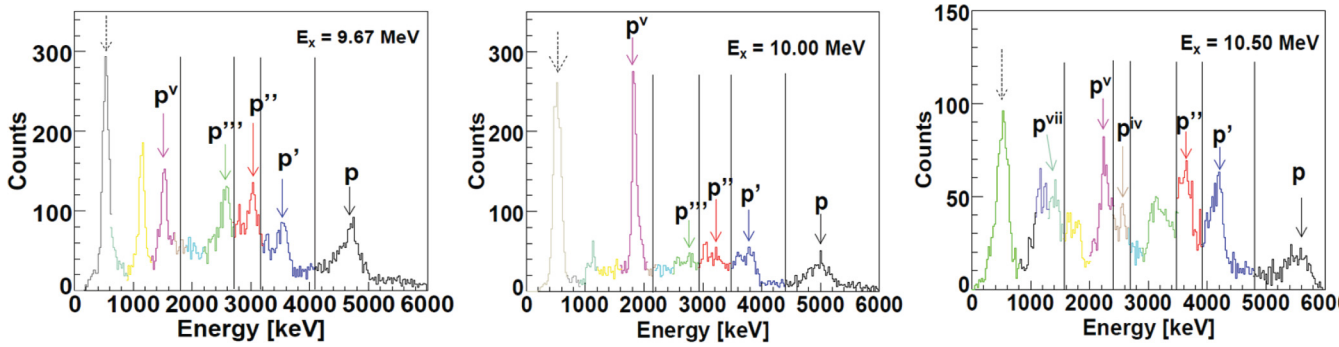

FIG. 7. (Color online) Event-by-event reconstructed spectra for different energy levels in ^{30}S above the α-decay threshold measured in the present ^{28}Si(^{3}He,n-p) experiment. The different colors separated by vertical lines correspond to the different kinematics used to reconstruct different portions of the spectra. The low-energy peak present in the spectra, marked by the dashed arrow, arises because of the presence of carbon contamination in the target. In some cases, contamination from neighboring energy levels is observed (unlabeled peaks). Branching ratios are listed in Table V.

previously reported states [17,19–22]. Bardayan *et al.* [10] quote only one level for this excitation range. Based on previous arguments about the mirror structure in the ^{30}S-^{30}Si system [10,15,19,35], we adopt a spin parity of 4^+ for the 5.130-MeV state and a spin parity of 0^+ for the state at 5.218 MeV. With these assignments, we assume the 5.130- and 5.218-MeV states to be the mirrors of the 5.280- and 5.372-MeV states in ^{30}Si. The doublet could not be resolved in our ^{28}Si(^{3}He,n) measurement. A proton decay in the range of 98%–100% was observed to the $1/2^+$ ground state of ^{29}P, which is most likely associated with the decay of the 0^+ state at 5.218 MeV.

The states observed at 5.3121 ± 0.0022, 5.3820 ± 0.0011, and 5.8355 ± 0.0016 MeV in the ^{32}S(p,t) spectra are believed to be the same as those observed previously [20] at 5.288, 5.425, and 5.912 MeV, respectively, and, more recently, at 5.318 and 5.396 MeV [22]. These states are assumed to be the mirrors of the levels in ^{30}Si found at 5.487, 5.614, and 5.950 MeV, respectively. Based on this mirror assignment, we adopt 3^- for the 5.312-MeV state, 2^+ for the level at 5.382 MeV, and 4^+ for the state at 5.836 MeV. The 2^+ level at 5.382 MeV is observed to decay 96%–100% to the ground state of ^{29}P. No significant proton decay is observed for the state at 5.836 MeV, which indicates that the proton decay is suppressed by a high-orbital-momentum barrier, supporting the 4^+ assignment in agreement with previous suggestions [20].

Previously observed levels in the excitation range between 6.0 and 6.3 MeV were not observed in the ^{32}S(p,t) spectra at the two angle positions of the spectrometer. However, the states are strongly populated by the ^{28}Si(^{3}He,n) reaction [20] and a 100% decay into the proton channel was observed. This observation is confirmed in the present work and the corresponding excitation energies have been determined to be 6.000 ± 0.041 and 6.240 ± 0.042 MeV.

The state observed at 6.3259 ± 0.0011 MeV in the ^{32}S(p,t) spectra corresponds to the level at 6.3386 MeV, which was previously identified in the β-delayed proton decay of ^{31}Ar [21] and at 6.393 MeV in the ^{28}Si(^{3}He,n-p)^{29}P analysis by Yokota *et al.* [20]. Based on these data a $J^\pi = 0^+$ assignment was suggested. This agrees well with the present results, where a large ^{32}S(p,t) cross section anisotropy between -0.3° and 8° also indicates a 0^+ assignment. This level, however, could not be clearly identified in the present ^{28}Si(^{3}He,n-p)^{29}P experiment owing to the limited statistics in the proton spectra. Based on the 0^+ spin-parity assignment, we assume this state to be the mirror of the 6.642-MeV state in ^{30}Si.

The state observed at 6.5121 ± 0.0034 MeV in the ^{32}S(p,t) experiment corresponds to the level at 6.541 MeV which was observed in the β-delayed proton decay of ^{31}Ar [21] and in the ^{28}Si(^{3}He,n-p)^{29}P experiment by Yokota *et al.* [20]. Again, the statistics in the present ^{28}Si(^{3}He,n-p)^{29}P experiment was not sufficient for a clear identification and energy assignment of this level. Since this level is clearly visible in the (p,t) reaction, which shows a preference for natural parity states, we tentatively assume this state to be the mirror of the 6.744-MeV 1^- level in ^{30}Si.

TABLE I. Energy levels below the charged-particle threshold in ^{30}S measured in the present experiments and comparison with previous results. Excitation energies are given in MeV. g.s., ground state.

This work		Bardayan *et al.* [10]		Paddock [17]:	Kuhlmann *et al.* [19]		Caraça *et al.* [18]:	Setoodehnia *et al.* [22]:
^{32}S(p,t)^{30}S	^{28}Si(^{3}He,n)^{30}S	^{32}S(p,t)^{30}S	J^π	^{32}S(p,t)^{30}S	^{28}Si(^{3}He,nγ)^{30}S	J^π	^{28}Si(^{3}He,nγ)^{30}S	^{32}S(p,t)^{30}S
g.s.	g.s.	0.000000(4)	0^+	g.s.				
2.2085(22)	2.20(21)	2.2107	2^+	2.239(18)	2.2107(5)	2	2.2099(11)	2.2106
3.4058(12)		3.4026	2^+	3.438(14)	3.4026(5)	1, 2	3.4022(13)	3.4026
	3.60(26)				3.6675(10)		3.6642(13)	
3.6773(70)		3.680(6)	(1^+)	3.707(25)	3.676(3)	1		3.680 (4)

TABLE II. Energy levels between the proton-decay threshold and the α-decay threshold in ^{30}S measured in the present experiments and comparison with previous results. Excitation energies are given in MeV.

This work			Fynbo *et al.* [21]:	Yokota *et al.* [20]		Bardayan *et al.* [10]		Paddock [17]:	Setoodehnia *et al.* [22]:
^{32}S(p,t)^{30}S	^{28}Si(^{3}He,np)^{30}S	J^{π}	^{31}Ar(β^{+})(p)^{30}S	^{28}Si(^{3}He,np)^{30}S	J^{π}	^{32}S(p,t)^{30}S	J^{π}	^{32}S(p,t)^{30}S	^{32}S(p,t)^{30}S
4.6825(57)						4.704(5)			4.693(5)
									4.814(3)
5.1300(18)		4^{+}		5.145		5.168(6)	$4^{+}+0^{+}$	5.207(22)	5.136
5.2178(28)	5.200(44)	0^{+}	5.2174(7)						5.226(3)
5.3121(20)		3^{-}		5.288	3^{-}			5.306(25)	5.318(4)
5.3820(7)	5.400(43)	2^{+}	5.389(2)	5.425	(1,2)	5.383(8)	$(3^{-}, 2^{+})$	5.426(25)	5.396(4)
5.8355(13)		4^{+}	5.842(4)	5.912	(3,4)	5.843(5)	(1^{-})	5.897(27)	
			(5.945(3))						
	6.000(41)		6.064(3)	6.117	1^{-}	6.071(11)		(6.108(29))	
	6.240(42)		6.202(3)	6.233				(6.223(30))	
			6.2801(12)						
6.3259(7)		0^{+}	6.3386(14)	6.393	0^{+}	6.341(5)		6.415(40)	
6.5121(33)		(1^{-})	6.541(4)	6.584	(2,3)	6.532(13)			
			(6.643(3))						
6.7375(7)	6.730(44)	2^{+}	6.762(4)	6.810		6.766(10)	2^{+}	6.861(40)	
			6.855(4)	6.838	$\geqslant 4$				
6.9015(23)		(1^{-})	6.927(4)	6.919	(3,4)				
7.0589(25)		0^{+}	7.078(7)	7.133	(1,2)	7.074(9)		7.185(35)	
			7.123(10)						
7.1949(18)	7.180(41)	3^{-}	(7.237(5))	7.294	$\geqslant 3$				
			7.295(14)						
7.3106(7)	7.330(44)	(2^{+})	7.352(8)	7.338	(1,2)				
7.4465(12)	7.420(45)	(4^{+})	7.485(4)	7.475					
			7.598(4)					7.570(45)	
			7.693(4)						
7.8990(8)	7.910(49)		7.924(5)						
8.0828(23)	8.060(51)								
8.4823(15)									
	8.680(44)								
8.8750(82)									
9.0806(45)									
9.2763(42)	9.220(41)								

The state observed at 6.737 MeV in the ^{32}S(p,t) experiment is thought to be identical to the state observed at 6.762 MeV in the β-delayed proton decay of ^{31}Ar [21]. The spin assignment is adopted to be 2^{+} [10], assuming it to be the mirror of the level at 6.915 MeV in ^{30}Si. The proton-decay spectrum has been measured in the present ^{28}Si(^{3}He,n-p)^{29}P study and suggests a $14\% \pm 4\%$ branch to the $1/2^{+}$ ground state in ^{29}P and a branch in the range of 70%–100% to the $3/2^{+}$ first-excited state at 1.384 MeV. This ratio reflects the difference in the orbital-momentum barrier for a d-wave decay to the ground state versus an s-wave decay to the first-excited state, which supports the above 2^{+} spin assignment.

The state observed at 6.901 MeV in the ^{32}S(p,t) experiment has not been reported before. However, it could correspond to the previously reported level at 6.927 MeV [21] or 6.919 MeV [20]. This level was not observed in the present ^{28}Si(^{3}He,n-p)^{29}P experiment owing to the limited statistics. Because the state is clearly populated in the (p,t) reaction, which preferably populates natural parity states, and owing to the very similar pattern observed in its population with the level observed at 6.512 MeV, we tentatively assign the spin parity (1^{-}).

The state at 7.059 MeV in the present ^{32}S(p,t) measurement was also observed by Bardayan *et al.* at 7.074 MeV [10] as the state of the highest excitation energy covered in that study. This energy agrees well with the results from the β-delayed proton decay of ^{31}Ar, which assigned a value of 7.078 MeV [21]. This state exhibits a high ^{32}S(p,t) cross-section ratio between -0.3° and 8°, suggesting a spin-parity assignment of 0^{+}. The proton decay of this state could not be observed in the present ^{28}Si(^{3}He,n-p)^{29}P experiment.

The state observed at 7.1949 ± 0.0020 MeV is thought to be identical to the tentatively identified level at 7.237 MeV [21] or 7.294 MeV [20]. It was also observed in the present ^{28}Si(^{3}He,n-p)^{29}P study, yielding a proton-decay branching of $28\% \pm 5\%$ to the ground state, $64\% \pm 7\%$ to the $3/2^{+}$ first-excited state, and $8\% \pm 2\%$ to the $5/2^{+}$ second-excited state at 1.954 MeV. While previous results suggest a spin of $\geqslant 3$, the observed proton-decay branching ratios match best with an f-wave transition to the ground state and a p-wave transition

TABLE III. Summary of results obtained from the energy levels in ^{30}S between the proton-decay threshold and the α-decay threshold in the present ^{28}Si(^{3}He,n-p) experiment. Excitation energies, branching ratios (BR), and partial widths are listed.

^{30}S E_x (MeV)	BR	Partial width
5.200 ± 0.044	$BR_p = 1.00 \pm 0.02$	
5.400 ± 0.043	$BR_p = 1.00 \pm 0.04$	
6.000 ± 0.041	$BR_p = 1.00 \pm 0.02$	
6.240 ± 0.042	$BR_p = 1.00 \pm 0.06$	
6.730 ± 0.044	$BR_p = 0.14 \pm 0.04$	
	$BR_{p'} = 0.86 \pm 0.16$	$\frac{\Gamma_{p'}}{\Gamma_p} = 6.14$
7.180 ± 0.041	$BR_p = 0.28 \pm 0.05$	
	$BR_{p'} = 0.64 \pm 0.07$	$\frac{\Gamma_{p'}}{\Gamma_p} = 2.29$
	$BR_{p''} = 0.08 \pm 0.02$	$\frac{\Gamma_{p''}}{\Gamma_p} = 0.29$
7.330 ± 0.044	$BR_p = 0.63 \pm 0.05$	
	$BR_{p''} = 0.37 \pm 0.09$	$\frac{\Gamma_{p''}}{\Gamma_p} = 0.59$
7.420 ± 0.045	$BR_p = 0.37 \pm 0.08$	
	$BR_{p'} = 0.43 \pm 0.06$	$\frac{\Gamma_{p'}}{\Gamma_p} = 1.16$
	$BR_{p''} = 0.20 \pm 0.04$	$\frac{\Gamma_{p''}}{\Gamma_p} = 0.54$
7.910 ± 0.049	$BR_p = 0.58 \pm 0.10$	
	$BR_{p''} = 0.38 \pm 0.25$	$\frac{\Gamma_{p''}}{\Gamma_p} = 0.65$
	$BR_{p'''} = 0.04 \pm 0.02$	$\frac{\Gamma_{p'''}}{\Gamma_p} = 0.07$
8.060 ± 0.051	$BR_p = 0.48 \pm 0.05$	
	$BR_{p'} = 0.17 \pm 0.07$	$\frac{\Gamma_{p'}}{\Gamma_p} = 0.35$
	$BR_{p''} = 0.25 \pm 0.10$	$\frac{\Gamma_{p''}}{\Gamma_p} = 0.52$
	$BR_{p'''} = 0.10 \pm 0.08$	$\frac{\Gamma_{p'''}}{\Gamma_p} = 0.21$
8.680 ± 0.044	$BR_p = 0.10 \pm 0.02$	
	$BR_{p'} = 0.25 \pm 0.08$	$\frac{\Gamma_{p'}}{\Gamma_p} = 2.5$
	$BR_{p''} = 0.24 \pm 0.08$	$\frac{\Gamma_{p''}}{\Gamma_p} = 2.4$
	$BR_{p'''} = 0.03 \pm 0.01$	$\frac{\Gamma_{p'''}}{\Gamma_p} = 0.3$
	$BR_{p^v} = 0.38 \pm 0.10$	$\frac{\Gamma_{p^v}}{\Gamma_p} = 3.8$
9.220 ± 0.041	$BR_p = 0.10 \pm 0.03$	
	$BR_{p'} = 0.19 \pm 0.06$	$\frac{\Gamma_{p'}}{\Gamma_p} = 1.9$
	$BR_{p''} = 0.23 \pm 0.05$	$\frac{\Gamma_{p''}}{\Gamma_p} = 2.3$
	$BR_{p'''} = 0.06 \pm 0.02$	$\frac{\Gamma_{p'''}}{\Gamma_p} = 0.6$
	$BR_{p^v} = 0.42 \pm 0.08$	$\frac{\Gamma_{p^v}}{\Gamma_p} = 4.2$

to the two first-excited states in ^{29}P; we therefore suggest a 3^- spin-parity assignment for this level.

Two pronounced levels were also observed at energies of 7.3106 and 7.4465 MeV in the ^{32}S(p,t) spectra, which correspond to a cluster of states observed in the β-delayed proton decay of ^{31}Ar [21]. These states are also observed in the ^{28}Si(^{3}He,n-p)^{29}P proton spectra; the first level shows a proton-decay branching of 63% ± 5% to the ground state and 37% ± 9% to the second-excited state in ^{29}P. The transition to the first-excited state is rather weak and could not be resolved owing to contaminations from the decay of neighboring levels. This resembles a rather odd decay pattern most likely coming from an unresolved doublet with the lower spin component decaying preferably to the $1/2^+$ ground state in ^{29}P, while the level with the higher spin value decays to the $5/2^+$ second-excited state in ^{29}P. The mirror states in ^{30}Si could be the 2^+ and the 4^+ states at 7.623 and 7.810 MeV, respectively. The 7.446-MeV state was identified in the proton spectrum with an energy of 7.42 MeV and a 37% ± 8% decay to the ground state, 43 ± 6% to the first-excited state, and 20% ± 4% to the second-excited state in ^{29}P. Again, this probably reflects the decay pattern of an unresolved doublet configuration corresponding to a cluster of 2^+ and 4^+ states near 8.0 MeV in the mirror nucleus ^{30}Si.

The ^{32}S(p,t) spectra also indicate a strong transition to a state at 7.899 MeV, with a second weakly populated level at 8.08 MeV. The proton decay of both configurations has been observed in the ^{28}Si(^{3}He,n-p)^{29}P experiment, which suggests excitation energies of 7.91 and 8.06 MeV. The 7.91-MeV level decays primarily by 58% ± 10% to the ground state and 38% ± 25% to the second-excited state, with a third weak transition of 4% ± 2% to the $3/2^+$ third-excited state at 2.423 MeV in ^{29}P. A similar complex decay pattern is observed for the level configuration near 8.06 MeV, with a 48% ± 5% decay to the ground state, a 17% ± 7% decay to the first-excited state, a 25% ± 10% branch to the second-excited state, and, finally, a weak, 10% ± 8% decay to the third-excited state. Again, orbital-momentum transfer arguments exclude that this could reflect the decay pattern of a single level, and it is probably associated with the decay of a number of unresolved states in the excitation range near 8.0 MeV in ^{30}S. Indeed, the level structure in the corresponding excitation energy range in the mirror nucleus ^{30}Si is characterized by a cluster of 1^-, 2^+, and 5^- states near 8.2 MeV and a second group of 3^- and 4^+ states near 8.5 MeV, which could explain the complex proton-decay pattern through a mixture of orbital momenta as observed.

Further level configurations near the α threshold were discovered in the ^{32}S(p,t) spectra at 8.482 and 8.875 MeV. Corresponding to that energy range the ^{28}Si(^{3}He,n-p)^{29}P proton spectra indicate the decay of an 8.68-MeV configuration to the ground state, the first three excited states, and the $7/2^+$ fifth-excited state in ^{29}P. A similar decay pattern is observed for the configuration at 9.22 MeV, which was also identified in the ^{32}S(p,t) spectrum with levels at 9.081- and 9.276-MeV excitation energy. Again, the mirror nucleus shows, in the corresponding excitation range, a rather high level density, which corresponds to a large number of states in ^{30}S reflected in the collective proton decay of unresolved states populated in the ^{28}Si(^{3}He,n-p) transfer reaction.

C. α-unbound states in ^{30}S above 9.343 MeV

A number of α-unbound states were observed for the first time in the present experiments. Similarly to the case of proton-unbound states, some levels were observed in both experiments while some were detected in only one experiment and not the other. The excitation energies were determined for all observed levels and are listed in Table IV.

For the 20 states observed in the ^{32}S(p,t)^{30}S experiment in this energy region, the states measured at 9.3914 ± 0.0065, 9.7012 ± 0.0056, and 9.8742 ± 0.0091 MeV have cross-section ratios of 3 to 5 between the angles of -0.3° and 8°.

TABLE IV. Energy levels above the α-decay threshold at $E_x = 9.343$ MeV in ^{30}S measured in the present experiments. Excitation energies are given in MeV.

^{32}S(p,t)^{30}S	^{28}Si(^{3}He,np)^{30}S	J^π
9.3914(65)		$(0^+, 1^-, 2^+)$
9.4860(74)		
9.7012(56)	9.670(41)	$(0^+, 1^-, 2^+)$
9.7851(44)		
9.8742(91)		$(0^+, 1^-, 2^+)$
10.0088(208)	10.000(41)	
10.0705(55)		
10.1226(15)		
10.2747(19)		
10.4431(46)	10.500(43)	
	10.650(43)	
10.7551(30)		
10.8149(28)	10.830(40)	
11.0154(8)	11.000(35)	
	11.100(35)	
	11.200(32)	
	11.300(32)	
11.3997(22)	11.380(26)	
11.4904(33)	11.450(24)	
11.5462(20)	11.560(23)	
11.6091(25)	11.620(26)	
11.6817(40)	11.710(20)	
	11.770(19)	
11.8523(37)	11.860(20)	
12.0392(23)		

This suggests an angular momentum of $\leqslant 2$ and spin parities of 0^+, 1^-, or 2^+.

In the ^{28}Si(^{3}He,n-p)^{29}P experiment a total of 16 states above the α-decay threshold were measured. Branching ratios were extracted for three levels, located at $E_x = 9.670 \pm 0.041$ MeV, $E_x = 10.000 \pm 0.041$ MeV, and $E_x = 10.500 \pm 0.043$ MeV. The results for the branching ratios measured for these levels are listed in Table V. For the remaining 13 states the branching ratios were not measured because the energy of the proton decaying to the ground state of ^{29}P is outside the range of the silicon detectors (6 MeV).

In the present experiments, no spin assignment could be made for the observed α-unbound states at energies above 10 MeV. The resonance states above the α-decay threshold would be relevant in the calculation of the astrophysically important ^{26}Si(α,p)^{29}P reaction rate.

D. The level structure of ^{30}S

The tentative spin assignments were made using all available experimental information of this work. Owing to the high centrifugal barriers we assume that the spins of the states are generally between 0 and 4. From the (p,t) data, the ratio of the cross sections at -0.3° and 8° is generally high for the population of 0^+ and 2^+ states (this ratio is 2.7 for the case of the 0^+ ground state of ^{30}S and 1.5 for the 2^+ first excited state). Therefore, the ratio of the cross sections taken at these different

TABLE V. Summary of states observed in ^{30}S above the α-decay threshold at $E_x = 9.343$ MeV measured in the present ^{28}Si(^{3}He,n-p) experiment for which the branching ratios were measured. Excitation energies, branching ratios (BR), and partial widths are provided.

^{30}S E_x (MeV)	BR	Partial width
9.670 ± 0.041	$\mathrm{BR}_p = 0.13 \pm 0.03$	
	$\mathrm{BR}_{p'} = 0.17 \pm 0.06$	$\frac{\Gamma_{p'}}{\Gamma_p} = 1.31$
	$\mathrm{BR}_{p''} = 0.23 \pm 0.06$	$\frac{\Gamma_{p''}}{\Gamma_p} = 1.77$
	$\mathrm{BR}_{p'''} = 0.20 \pm 0.07$	$\frac{\Gamma_{p'''}}{\Gamma_p} = 7.54$
	$\mathrm{BR}_{p^v} = 0.27 \pm 0.05$	$\frac{\Gamma_{p^v}}{\Gamma_p} = 2.08$
10.000 ± 0.041	$\mathrm{BR}_p = 0.11 \pm 0.05$	
	$\mathrm{BR}_{p'} = 0.12 \pm 0.06$	$\frac{\Gamma_{p'}}{\Gamma_p} = 1.01$
	$\mathrm{BR}_{p''} = 0.11 \pm 0.06$	$\frac{\Gamma_{p''}}{\Gamma_p} = 1.0$
	$\mathrm{BR}_{p'''} = 0.10 \pm 0.07$	$\frac{\Gamma_{p'''}}{\Gamma_p} = 0.91$
	$\mathrm{BR}_{p^v} = 0.56 \pm 0.10$	$\frac{\Gamma_{p^v}}{\Gamma_p} = 5.09$
10.500 ± 0.043	$\mathrm{BR}_p = 0.04 \pm 0.01$	
	$\mathrm{BR}_{p'} = 0.26 \pm 0.08$	$\frac{\Gamma_{p'}}{\Gamma_p} = 6.5$
	$\mathrm{BR}_{p''} = 0.30 \pm 0.09$	$\frac{\Gamma_{p''}}{\Gamma_p} = 7.5$
	$\mathrm{BR}_{p^{iv}} = 0.08 \pm 0.03$	$\frac{\Gamma_{p^{iv}}}{\Gamma_p} = 2.0$
	$\mathrm{BR}_{p^v} = 0.19 \pm 0.06$	$\frac{\Gamma_{p^v}}{\Gamma_p} = 4.75$
	$\mathrm{BR}_{p^{vii}} = 0.13 \pm 0.04$	$\frac{\Gamma_{p^{vii}}}{\Gamma_p} = 3.25$

angles can be used to constrain the set of possible spins. Typical ratios for specific spin values have been taken from levels with previously confirmed spin assignments. The calculated proton widths are used to discard spin assignments that imply proton widths larger than the experimentally measured ones. The experimentally measured widths of the states as well as the proton partial widths were also used to constrain the spins of the levels in ^{30}S by comparing them with the calculated values.

The calculation of the proton partial widths Γ_p was done using the expression

$$\Gamma_p = C^2 S \Gamma_{\mathrm{sp}}, \tag{1}$$

where C^2S is the spectroscopic factor and Γ_{sp} denotes the partial width of a single-particle resonance located at the same energy as the resonance of interest [34]. The partial widths Γ_{sp} were computed using the code DWUCK4 [36]. In the determination of the partial widths Γ_{sp} using DWUCK4 it is necessary to specify the quantum number N (number of nodes of the wave function) and the angular momentum ℓ for the resonance state. Using shell model calculations it is possible to determine which orbital may be populated by the valence protons given the number of protons in the core and, therefore, determining n and ℓ for that state where $N = n - 1$. In the calculation of the spin and angular momentum transfer of the $^{29}\mathrm{P} + \mathrm{p}$ system, it was assumed that they couple to the state of minimum spin and angular momentum available. When possible, the spectroscopic factors were assumed from the corresponding mirror states. In the absence of spectroscopic factor information, values of 0.1 for C^2S were assumed for states below the α-decay threshold and 0.01 for states above it.

The widths of the states were extracted from the experimental data and compared with the calculated values. The resolution of the ^{32}S(p,t) experiment is better than that of the ^{28}Si(^{3}He,n) experiment, so we used the (p, t) set of data to measure the widths of the states whenever the states in (^{3}He,n) data matched the energy of states in the (p,t) data. The measured intrinsic width of the ^{32}S(p,t) data is $\Gamma_{\rm int} = 45 \pm 5$ keV, while the measured intrinsic width of the ^{28}Si(^{3}He,n) is $\Gamma_{\rm int} = 70 \pm 10$ keV. The total measured widths of the states were extracted using the relation $\Gamma = \sqrt{\Gamma^2_{\rm meas} - \Gamma^2_{\rm int}}$. After constraining the spin assignments of the resonant levels, we calculated the corresponding γ or α widths to be used in the calculations of the (p,γ) or (α,p) reaction rates. The γ widths needed for the (p,γ) reaction rates were calculated based on the lifetimes of the mirror states, when possible. In the absence of experimental information, the γ widths were calculated using "average γ transition strengths" [5]. Only the most probable transitions (E1, M1, and E2) were used in the calculations of the γ widths according to the expressions

$$\Gamma_\gamma({\rm M1}) = 10^{-1.25} 2.1 \times 10^{-2} E_\gamma^3, \tag{2}$$

$$\Gamma_\gamma({\rm E1}) = 10^{-3.5} 6.8 \times 10^{-2} A^{2/3} E_\gamma^3, \tag{3}$$

$$\Gamma_\gamma({\rm E2}) = 10^{0.5} 4.9 \times 10^{-8} A^{4/3} E_\gamma^5, \tag{4}$$

where Γ_γ are the γ widths (eV), A is the mass of the nucleus (amu), and E_γ are the transition energies (MeV).

In the present experiments, states above the α-decay threshold in ^{30}S are measured for the first time. In order to provide tentative spin assignments for these energy levels, we compared the experimental information from the branching ratios of the ^{28}Si(^{3}He,n) data to the calculations for the proton partial and total widths to constrain the tentative spin assignments. In the case where no experimental branching ratios were obtained ($E_x \geqslant 10.5$ MeV) only the total proton widths were used for the tentative spin assignments. For energy levels above the α-decay threshold and after a tentative spin assignment, α widths were calculated using Eq. (1). The α widths were calculated using the DWUCK4 code [36]. The calculation of the quantum numbers needed to input in DWUCK4 is slightly more difficult than for the proton width calculations. In this case, a $^{26}{\rm Si} + \alpha$ system is considered. The quantum numbers N, number of nodes of the wave function, and $L = \ell$ relative angular momentum of the α particle are needed. As both the core (^{26}Si) and the α cluster have total spin equal to 0 in their ground states, the angular momentum L of the α particle must be equal to the spin of the resonant state in ^{30}S. Determination of the number of nodes of the wave function was done with the prescription given by Mohr using the Wildermuth condition [37]:

$$Q = 2N + L = \sum_{i=1}^{4} q_i, \tag{5}$$

where Q is the number of oscillator quanta, N is the number of nodes, L is the relative angular momentum of the α particle, and q_i are the corresponding quantum numbers of the nucleons in the α cluster. For the present case, $Q = \sum q_i = 8$ or 9 for states with even or odd spin, respectively. Knowing the values of Q and L, the value of N can be determined and the corresponding α width calculated.

For energy levels above $E_x = 10.5$ MeV, the branching ratios could not be measured because the energy in the silicon detectors of the corresponding proton decay to the ground state of ^{29}P is higher than 6 MeV, which is outside of our energy range. The proton widths and partial widths were calculated considering that the proton decay would populate excited states in ^{29}P up to the fifth-excited state, as was observed in most of the cases for lower-lying levels. In this way the total widths were calculated and compared with the measured values. This condition just excluded one, two, and, in a few cases, three possible spins; for example, in most cases spin 2 is excluded owing to the very large proton width, resulting from the calculations.

After all selections were made, if more than one spin state was still possible, the spin value used in the calculation of the ^{26}Si(α,p) reaction rate was randomly chosen.

V. ASTROPHYSICAL IMPLICATIONS

For both ^{29}P(p,γ)^{30}S and ^{26}Si(α,p)^{29}P the reaction rates are dominated by the resonant reaction contributions due to the fairly high level density in the ^{30}S compound nucleus. In particular, for radiative proton capture on ^{29}P it was demonstrated in earlier work [15,16] that the direct-capture component in the reaction rate is negligible. We, therefore, concentrate in the following on the resonant contributions to the reaction rate.

The resonant reaction rate was calculated using the expression for narrow, well-separated resonances [38,39],

$$N_A \langle \sigma \upsilon \rangle = 1.54 \times 10^{11} A^{-3/2} T_9^{-3/2} \times \sum_i \omega\gamma_i \exp\left(-\frac{11.605 E_i}{T_9}\right), \tag{6}$$

with A being the reduced mass (in amu), E_i the resonance energy in the center-of-mass system (in MeV), and T_9 the temperature (in units of GK). The resonance strength $\omega\gamma$ in MeV is defined as

$$\omega\gamma = \frac{2J+1}{(2I_1+1)(2I_2+1)} \times \frac{\Gamma_a \Gamma_b}{\Gamma}. \tag{7}$$

In the case of the ^{26}Si(α,p)^{29}P reaction, J, $I_1 = I_\alpha = 0$, and $I_2 = I_{^{26}{\rm Si}} = 0$ are the total angular momentum of the resonance, the α particle, and the ^{26}Si, respectively. $\Gamma_a = \Gamma_\alpha$ is the width of the α particle, while $\Gamma_b = \Gamma_{p_{\rm tot}} = \Gamma_p + \sum_i^7 \Gamma_{p^i}$ is the total proton width and Γ is the total width of the state.

In the case of the ^{29}P(p,γ)^{30}S reaction, J, $I_1 = I_p = 1/2$, and $I_2 = I_{^{29}P} = 1/2$ are the total angular momentum of the resonance, the proton, and the ^{29}P ground state, respectively. $\Gamma_a = \Gamma_{p_{\rm tot}} = \Gamma_p + \sum_i^7 \Gamma_{p^i}$ is the total proton width, $\Gamma_b = \Gamma_\gamma$ is the γ width, and Γ is the total width of the state.

The partial widths were calculated using the formalism and the nuclear structure assumptions outlined in the previous section and listed in Tables VI and VII. The resonance strengths were derived from these parameters. It should be

TABLE VI. Resonance parameters used in calculations of the ^{29}P(p,γ)^{30}S resonance reaction rate.

E_x (MeV)	E_{cm} (MeV)	J^π	C^2S	Γ_p (eV)	Γ_γ (eV)	$\omega\gamma$ (MeV)
4.6825	0.2835	3^+	0.04[a]	0.000023[a]	0.0049[a]	4.01×10^{-11}[a]
4.814	0.4150	2^+	0.11[a]	0.037[a]	0.0048[a]	2.61×10^{-9}[a]
5.130	0.7310	4^+	0.02	0.23	0.00793[b]	1.72×10^{-8}
5.2178	0.8188	0^+	0.01	15.898	0.01115[b]	2.79×10^{-9}
5.3121	0.9131	3^-	0.33	0.0033	0.01530[b]	4.75×10^{-9}
5.382	0.9830	2^+	0.06	8.0436	0.31333[b]	3.90×10^{-8}
5.8355	1.4365	4^+	0.001	0.00279	0.04387[b]	5.90×10^{-9}
6.00	1.6010	0^+	0.56	74 838	0.015	3.75×10^{-9}
6.24	1.8410	2^+	0.58	4 647.54	0.039[b]	4.84×10^{-8}
6.3259	1.9269	0^+	0.44	130 000	0.082	2.05×10^{-8}
6.5121	2.1131	1^-	0.25	52 241	0.047[b]	3.52×10^{-8}
6.7375	2.3385	2^+	0.1	3 489	0.0274	3.42×10^{-8}
6.9015	2.5025	1^-	0.1	45 300	0.021	1.57×10^{-8}
7.0589	2.6599	0^+	0.1	106 000	0.046	1.15×10^{-8}
7.1949	2.7959	3^-	0.1	2 849	0.026	4.55×10^{-8}
7.3106	2.9116	2^+	0.1	21 011	0.0387[b]	4.84×10^{-8}
7.4465	3.0475	4^+	0.1	568	0.0548[b]	1.12×10^{-7}
7.899	3.500	2^+[c]	0.1	66 872	0.582	7.27×10^{-7}
8.0828	3.6838	3^-[c]	0.1	32 749	0.042	7.35×10^{-8}
8.4823	4.0833	1^-[c]	0.1	2 670	0.127	9.52×10^{-8}
8.68	4.2810	4^+[c]	0.1	13 627	0.075	1.69×10^{-7}
8.875	4.4760	0^+[c]	0.1	156 800	0.166	4.15×10^{-8}
9.0806	4.6816	2^+[c]	0.1	70 700	0.186	2.32×10^{-7}
9.2763	4.8773	4^+[c]	0.1	34 258	0.114	2.56×10^{-7}

[a]From Setoodehnia *et al.* [22].
[b]Lifetimes from mirror states.
[c]Spin randomly chosen among possible values.

noted that the nuclear structure input parameters carry a large uncertainty since they are not experimentally determined but are based on assumptions of typical single-particle and α-cluster strength distributions in this particular mass and excitation range of even-even nuclei. The classical approach is to weigh the uncertainty range for each resonance with a factor of (0–1) [38]. Empirically, we assume an uncertainty within one order of magnitude for the spectroscopic input parameters. Recently an attempt was made to provide an improved quantification of the uncertainty range based on Monte Carlo simulations assuming a characteristic Porter-Thomas distribution for the spectroscopic factors [40]. While this seems to be a reasonable approach for midshell nuclei, it is not necessarily a valid assumption for closed-shell even-even nuclei, where the number of statistical configurations is limited and pronounced cluster configurations near the α threshold cannot be excluded. In view of the uncertainties associated with the single-particle and α-cluster configurations in ^{30}S we feel that the proposed Monte Carlo approach is insufficient to cover the potentially large uncertainty range of the estimate. In the following we discuss the rates and compare them with previous evaluations.

A. The ^{29}P(p,γ)^{30}S reaction rate

A total of 24 possible resonances listed in Table II have been included in the estimate of the ^{29}P(p,γ)^{30}S reaction rate but only the six states from 4.683 to 5.382 MeV, shown in Fig. 8, contribute significantly to the reaction rate. All other contributions are small and fall within the shaded area shown in the figure. The resonance parameters are listed in Table VI. The resonance strengths for the two states at 4.683 and 4.814 MeV are determined by their proton partial widths, which in turn depend on the single-particle spectroscopic factors adopted for these states [22]. For the higher energy resonances the strength depends primarily on the γ-decay strength, which in most cases was adopted from the mirror levels in ^{30}Si. The resonance reaction rates calculated in this work are compared to previous calculations in Fig. 9, where the rates are presented as ratios to the rate calculated by Iliadis *et al.* [16]. The rate predicted by the statistical model NON-SMOKER [41] is substantially higher than any of the rates based on experimental level information. Given the relatively limited level density in the ^{30}S compound nucleus below 9-MeV excitation energy, we rule out the statistical model as a viable theoretical approach in this mass range. At higher temperatures all experiment-based predictions are in reasonable agreement; they deviate toward lower temperatures. Early estimates by Wiescher Görres (1987) [15], and Iliadis *et al.* (2001) [16] show the largest deviation from the present results, which is due to uncertainties in the level structure in the compound nucleus ^{30}S, which handicapped their analysis. The later work of Bardayan *et al.* (2007) [10] and, more recently, of Setoodehnia *et al.* (2010) [22] shows good agreement

TABLE VII. Resonance parameters used in calculations of the ^{26}Si(α,p)^{29}P resonance reaction rate.

E_x (MeV)	E_{cm} (MeV)	$J^{\pi,a}$	$C^2S(\alpha)$	Γ_α (eV)	$C^2S(p)$	Γ_p (eV)	$\omega\gamma$ (MeV)
9.3914	0.0484	2^+	0.01	9.78×10^{-89}	0.01	9 200	4.89×10^{-94}
9.486	0.1430	1^-	0.01	2.87×10^{-45}	0.01	44 500	8.61×10^{-51}
9.7012	0.3582	2^+	0.01	3.30×10^{-24}	0.01	12 357	1.65×10^{-29}
9.7851	0.4421	0^+	0.01	1.38×10^{-19}	0.01	444 962	1.38×10^{-25}
9.8742	0.5312	2^+	0.01	2.00×10^{-17}	0.01	14 126	1.00×10^{-22}
10.0088	0.6658	4^+	0.01	3.90×10^{-16}	0.01	758.11	2.61×10^{-21}
10.0705	0.7275	0^+	0.01	3.24×10^{-12}	0.01	131 513	3.24×10^{-18}
10.1226	0.7796	4^+	0.01	3.59×10^{-14}	0.01	844.87	3.23×10^{-19}
10.2747	0.9317	2^+	0.01	4.63×10^{-10}	0.01	18 166	2.32×10^{-15}
10.4431	1.1001	3^-	0.01	6.28×10^{-9}	0.01	3 975	4.40×10^{-14}
10.65	1.307	3^-	0.01	3.53×10^{-7}	0.01	4 630	2.47×10^{-12}
10.7551	1.4121	3^-	0.01	1.92×10^{-6}	0.01	4 990	1.35×10^{-11}
10.8149	1.4719	4^+	0.01	3.13×10^{-7}	0.01	1 545	2.82×10^{-12}
11.0154	1.6724	4^+	0.01	4.41×10^{-6}	0.01	1 812	3.97×10^{-11}
11.10	1.757	3^-	0.01	1.62×10^{-4}	0.01	6 296	1.14×10^{-9}
11.20	1.857	3^-	0.01	4.61×10^{-4}	0.01	6 708	3.23×10^{-9}
11.30	1.957	4^+	0.01	9.18×10^{-5}	0.01	2 250	8.26×10^{-10}
11.3997	2.0567	4^+	0.01	2.28×10^{-4}	0.01	2 421	2.05×10^{-9}
11.4904	2.1474	4^+	0.01	4.94×10^{-4}	0.01	2 586	4.45×10^{-9}
11.5462	2.2032	1^-	0.01	1.59×10^{-1}	0.01	3 964	4.77×10^{-7}
11.6091	2.2661	4^+	0.01	1.27×10^{-3}	0.01	2 813	1.14×10^{-8}
11.6817	2.3387	3^-	0.01	2.60×10^{-2}	0.01	8 854	1.82×10^{-7}
11.77	2.427	4^+	0.01	4.05×10^{-3}	0.01	3 146	3.64×10^{-8}
11.8523	2.5093	3^-	0.01	8.07×10^{-2}	0.01	9 660	5.65×10^{-7}
12.0392	2.6962	0^+	0.01	4.84×10^{0}	0.01	24 889	4.84×10^{-6}

[a]Spin randomly chosen among possible values.

within a factor of 2 but is lower than the present prediction at temperatures $T \leqslant 0.25$ GK. This is primarily caused by the revised excitation energy of the lowest resonance state, which is also supported by the recent in-beam γ spectroscopy study by Setoodehnia *et al.* (2011) [35].

The total resonance reaction rate calculated in the present work is reported in Table VIII in comparison with the resonance reaction rate proposed by Iliadis *et al.* [16].

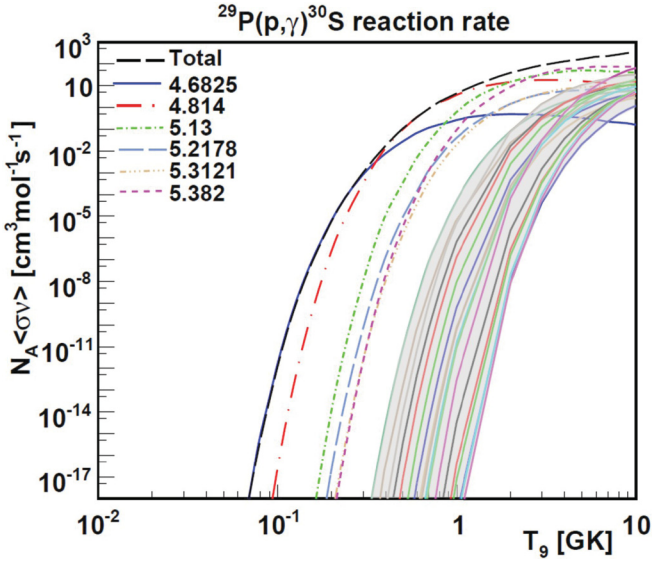

FIG. 8. (Color online) Contribution of the most relevant resonances to the ^{29}P(p,γ)^{30}S reaction rate. All other resonances listed in Table VI fall within the shaded area and make a limited contribution to the reaction rate.

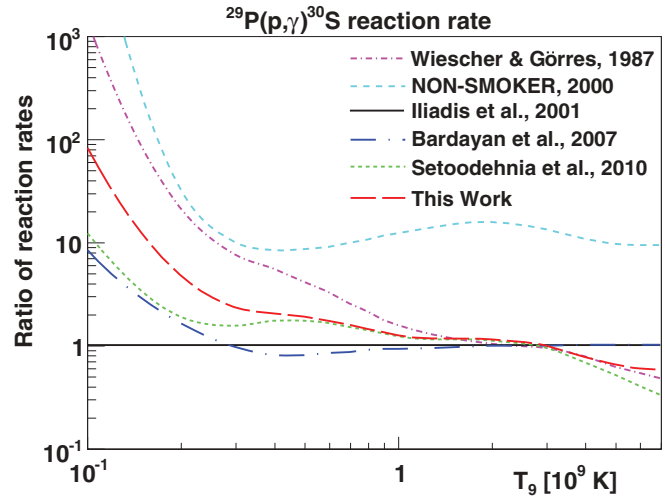

FIG. 9. (Color online) Resonance contribution to the ^{29}P(p,γ)^{30}S reaction rate calculated in this work and comparison with previous works. Reaction rates are plotted as ratios to the rate calculated by Iliadis *et al.* [16].

TABLE VIII. ^{29}P(p,γ)^{30}S and ^{26}Si(α,p)^{29}P resonance reaction rates calculated in this work and comparison with previous calculations.

T_9	^{29}P(p,γ)^{30}S reaction rate		^{26}Si(α,p)^{29}P reaction rate				
	This work	Iliadis *et al.* [16]	This work	SMOKER [49]	NON-SMOKER [50]	TALYS [51]	CIGAR [52]
0.1	1.06×10^{-12}	1.27×10^{-14}	1.66×10^{-35}	1.09×10^{-34}	2.93×10^{-34}		1.08×10^{-34}
0.15	3.34×10^{-8}	2.71×10^{-9}	1.44×10^{-28}	1.38×10^{-27}	2.30×10^{-27}	1.24×10^{-30}	1.47×10^{-27}
0.2	5.37×10^{-6}	1.11×10^{-6}	1.78×10^{-24}	3.26×10^{-23}	5.05×10^{-23}	4.36×10^{-24}	3.18×10^{-23}
0.25	1.15×10^{-4}	3.85×10^{-5}	1.84×10^{-21}	3.88×10^{-20}	6.14×10^{-20}	3.43×10^{-20}	
0.3	9.57×10^{-4}	4.04×10^{-3}	3.83×10^{-19}	8.36×10^{-18}	1.37×10^{-17}	1.30×10^{-17}	7.28×10^{-18}
0.35	4.75×10^{-3}	2.20×10^{-3}	2.40×10^{-17}	6.02×10^{-16}	1.02×10^{-15}		
0.4	1.68×10^{-2}	8.13×10^{-3}	6.81×10^{-16}	2.04×10^{-14}	3.56×10^{-14}	2.50×10^{-14}	1.64×10^{-14}
0.5	1.04×10^{-1}	5.47×10^{-2}	1.15×10^{-13}	5.13×10^{-12}	9.35×10^{-12}	5.76×10^{-12}	4.61×10^{-12}
0.6	3.60×10^{-1}	2.08×10^{-1}	5.72×10^{-12}	3.45×10^{-10}	6.43×10^{-10}	4.15×10^{-10}	3.35×10^{-10}
0.7	8.72×10^{-1}	5.58×10^{-1}	1.41×10^{-10}	9.85×10^{-9}	1.86×10^{-8}	1.18×10^{-8}	9.85×10^{-9}
0.8	1.69	1.18	2.21×10^{-9}	1.56×10^{-7}	2.95×10^{-7}	1.81×10^{-7}	1.56×10^{-7}
0.9	2.85	2.14	2.57×10^{-8}	1.59×10^{-6}	3.01×10^{-6}	1.81×10^{-6}	1.60×10^{-6}
1.0	4.37	3.47×10^{1}	2.32×10^{-7}	1.17×10^{-5}	2.21×10^{-5}	1.31×10^{-5}	1.17×10^{-5}
1.5	1.75×10^{1}	1.53×10^{1}	4.25×10^{-4}	1.25×10^{-2}	2.28×10^{-2}	1.28×10^{-2}	1.22×10^{-2}
2.0	3.85×10^{1}	3.37×10^{1}	2.38×10^{-2}	9.15×10^{-1}	1.61	8.68×10^{-1}	8.96×10^{-1}
2.5	6.28×10^{1}	5.74×10^{1}	2.75×10^{-1}	1.79×10^{1}	3.06×10^{1}	1.58×10^{1}	1.77×10^{1}
3.0	8.68×10^{1}	8.76×10^{1}	1.40	1.63×10^{2}	2.71×10^{2}	1.34×10^{2}	1.63×10^{2}
3.5	1.09×10^{2}	1.24×10^{2}	4.39	9.09×10^{2}	1.47×10^{3}	6.96×10^{2}	9.16×10^{2}
4.0	1.29×10^{2}	1.66×10^{2}	1.02×10^{1}	3.60×10^{3}	5.67×10^{3}	2.56×10^{3}	3.64×10^{3}
5.0	1.64×10^{2}	2.53×10^{2}	3.18×10^{1}	2.89×10^{4}	4.34×10^{4}	1.76×10^{4}	2.91×10^{4}
6.0	1.97×10^{2}	3.33×10^{2}	6.52×10^{1}	1.30×10^{5}	1.88×10^{5}	6.69×10^{4}	1.29×10^{5}
7.0	2.31×10^{2}	3.98×10^{2}	1.05×10^{2}	4.04×10^{5}	5.66×10^{5}	1.76×10^{5}	3.99×10^{5}
8.0	2.66×10^{2}	4.47×10^{2}	1.47×10^{2}	9.77×10^{5}	1.34×10^{6}	3.59×10^{5}	9.62×10^{5}
9.0	3.00×10^{2}	4.81×10^{2}	1.87×10^{2}	1.97×10^{6}	2.70×10^{6}	6.18×10^{5}	1.96×10^{6}
10.0	3.34×10^{2}	5.03×10^{2}	2.23×10^{2}	3.47×10^{6}	4.83×10^{6}	9.37×10^{5}	3.50×10^{6}

B. The ^{26}Si(α,p)^{29}P reaction rate

Present simulations of the αp process rely on statistical model predictions for the ^{26}Si(α,p)^{29}P reaction rate. States in ^{30}S above the α threshold have not been observed prior to this work. Yet the level structure and the level decay channels are not known and the derivation of the resonance strengths, therefore, carries large uncertainties. We assume only a small α-cluster configuration represented by the spectroscopic factor $C^2S_\alpha = 0.01$. The single-particle strength of levels at this high excitation energy is also assumed to be lower and we adopted a single-particle spectroscopic factor $C^2S_p = 0.01$. In all cases the α partial width is considerably smaller than the proton partial width and, therefore, determines the resonance strength distribution. In lighter, $T = 1$ nuclei such as ^{18}O, ^{22}Ne, and ^{26}Mg, pronounced α-cluster configurations above the α-decay threshold have been observed [42–48]. Therefore, the possibility of much higher resonance strengths cannot be excluded. A total of 25 resonances were considered for contributing to the reaction rate of ^{26}Si(α,p)^{29}P. The resonance parameters are listed in Table VII. The spins of the resonances were randomly chosen among the possible values as discussed in Sec. IV D. To estimate the uncertainty in this random approach, the reaction rate was calculated using a different set of spins. We found that the ^{26}Si(α,p)^{29}P reaction rate varies up to a factor of 10 when a different set of spins is chosen.

Many resonances contribute to the total reaction rate shown in Fig. 10. The figure also shows the reaction rates calculated using the statistical models SMOKER [49], NON-SMOKER [50], TALYS [51], and CIGAR [52], which are typically used to calculate this reaction rate.

The Hauser-Feshbach rates agree with each other within less than an order of magnitude, depending on the specific treatment for excitation energy and deformation dependence of level densities. The reaction rates predicted by the different Hauser-Feshbach calculations are listed in Table VIII in

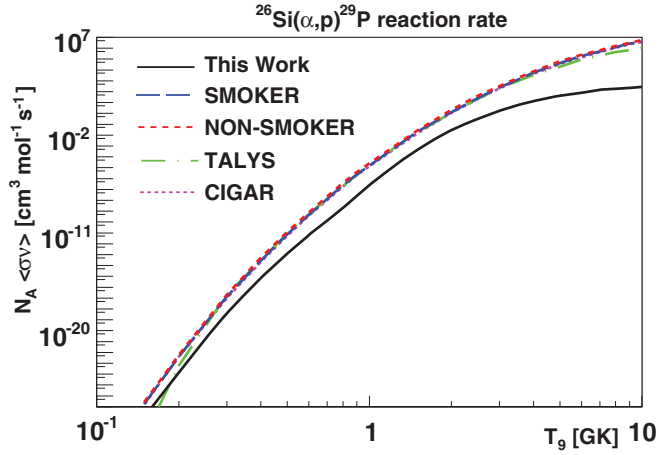

FIG. 10. (Color online) Resonance contribution to the ^{26}Si(α,p)^{29}P reaction rate calculated using the parameters listed in Table VII and comparison with the rates calculated using the statistical codes SMOKER [49], NON-SMOKER [50], TALYS [51] and CIGAR [52].

comparison with the rate predicted on the basis of the experimental data.

All of the statistical rates are substantially higher than the rate based on the observed resonance structure. Using the code CIGAR [52] we examined the sensitivity of the calculated reaction rate to both the radius and the diffuseness of the real and imaginary components of the α optical potential model. We find that increasing the real and imaginary radius and diffuseness by a factor of 1.086 reduces the reaction rate by up to a factor of $\sim$3. This result highlights the critical need for a better understanding of the α optical potential.

The reaction rate scales directly with the resonance strengths, which in turn depend on the α strengths. We have tested the impact of possible α-cluster states near the α threshold by increasing the strengths of resonances inside the Gamov window by two orders of magnitude. This causes an enhancement in a relative narrow temperature range corresponding to the excitation energy of the resonance level but has a limited effect on the overall reaction rate over the entire temperature range. It is clear that the question of the α-strength distribution in this excitation energy range and its impact on the reaction rate require more detailed studies of the ^{30}S compound nucleus at higher energies.

VI. CONCLUSIONS

The present work has focused on the nuclear level structure in ^{30}S and the consequences for the resonant contributions to the reaction cross sections of the ^{29}P(p,γ)^{30}S radiative capture and the ^{26}Si(α,p)^{29}P nuclear reaction process. Both reactions play a key role in the rp process and the αp process in explosive hydrogen burning [9,14]. The experiments helped to improve existing information on previously observed levels, but in addition, a large number of levels up to high excitation energies have been observed for the first time. The high resolution of the Grand Raiden spectrometer reduced substantially the uncertainty in the excitation and resonance energies of the populated states, removing one of the main obstacles to determining accurate reaction rates. The proton-decay studies provided additional information and constraint for the spin-parity assignments of the observed states. The reaction-rate calculation requires detailed information on the specific partial widths of the contributing resonance levels, namely, the proton partial widths of the low-energy resonances in ^{29}P(p,γ)^{30}S and the α partial widths of the resonances in ^{26}Si(α,p)^{29}P. These parameters are based on empirical quasistatistical assumptions about the single-particle and the α-cluster strength distribution in ^{30}S. While strong single-resonance contributions from pronounced single-particle states or cluster configurations cannot be excluded, the high resonance density reduces the overall impact of such pronounced resonance structures on the reaction rate.

ACKNOWLEDGMENTS

The authors are grateful for the support and help of the technical staff of the Notre Dame Nuclear Science Laboratory and the RCNP cyclotron facility at Osaka, Japan, during the course of the experiments. This work was supported by the NSF through Grant Nos. PHY0822648 and PHY0758100, the US Department of Energy through Grant Nos. DE-FG02-88ER40387 and DE-FG52-09NA29455, and JINA Grant No. PHY1068192.

[1] R. K. Wallace and S. E. Woosley, Astrophys. J. Suppl. Ser. **45**, 389 (1981).
[2] L. Van Wormer *et al.*, Astrophys. J. **432**, 326 (1994).
[3] H. Schatz *et al.*, Phys. Rev. Lett. **79**, 3845 (1997).
[4] S. Starrfield *et al.*, Nucl. Phys. A **621**, 495 (1997).
[5] M. Wiescher, J. Görres, F.-K. Thielemann, and H. Ritter, Astron. Astrophys. **160**, 56 (1986).
[6] C. Iliadis, A. E. Champagne, J. José, S. Starrfield, and P. Tupper, Astrophys. J. Suppl. Ser. **142**, 105 (2002).
[7] E. Zinner, Annu. Rev. Earth Planet Sci. **26**, 147 (1998).
[8] S. Amari, X. Gao, L. R. Nittler, E. Zinner, J. Jose, M. Hernanz, and R. S. Lewis, Astrophys. J. **551**, 1065 (2001).
[9] J. José, M. Hernanz, S. Amari, K. Lodders, and E. Zinner, Astrophys. J. **612**, 414 (2004).
[10] D. W. Bardayan *et al.*, Phys. Rev. C **76**, 045803 (2007).
[11] M. Sztajno *et al.*, Astrophys. J. **299**, 487 (1985).
[12] W. Penninx, E. Damen, J. Van Paradijs, and W. H. G. Lewin, Astron. Astrophys. **208**, 146 (1989).
[13] E. Kuulkers *et al.*, Astron. Astrophys. **382**, 947 (2002).
[14] J. L. Fisker, F.-K. Thielemann, and M. Wiescher, Astrophys. J. **608**, L61 (2004).
[15] M. Wiescher and J. Görres, Z. Phys. A **329**, 121 (1988).
[16] C. Iliadis, J. M. D'Auria, S. Starrfield, W. J. Thompson, and M. Wiescher, Astrophys. J. Suppl. Ser. **134**, 151 (2001).
[17] R. A. Paddock, Phys. Rev. C **5**, 485 (1972).
[18] J. M. G. Caraça, R. D. Gill, A. J. Cox, and H. J. Tose, Nucl. Phys. A **193**, 1 (1972).
[19] E. Kuhlmann, W. Albrecht, and A. Hoffmann, Nucl. Phys. A **213**, 82 (1973).
[20] H. Yokota, K. Fujioka, K. Ichimaru, Y. Mihara, and R. Chiba, Nucl. Phys. A **383**, 298 (1982).
[21] H. O. U. Fynbo *et al.*, Nucl. Phys. A **677**, 38 (2000).
[22] K. Setoodehnia *et al.*, Phys. Rev. C **82**, 022801(R) (2010).
[23] A. Matic *et al.*, Phys. Rev. C **84**, 025801 (2011).
[24] A. Matic *et al.*, Phys. Rev. C **80**, 055804 (2009).
[25] A. Matic *et al.*, Phys. Rev. C **82**, 025807 (2010).
[26] G. Audi, O. Bersillon, J. Blachot, and A. H. Wapstra, Nucl. Phys. A **729**, 3 (2003).
[27] J. Souin, T. Eronen, P. Ascher, L. Audirac, J. Äystö, B. Blank, V.-V. Elomaa, J. Giovinazzo, J. Hakala, A. Jokinen, V. S. Kolhinen, P. Karvonen, I. D. Moore, S. Rahaman, J. Rissanen, A. Saastamoinen, and J. C. Thomas, Eur. Phys. J. A **47**, 40 (2011).
[28] M. Fujiwara *et al.*, Nucl. Instrum. Methods Phys. Res. Sec. A **422**, 484 (1999).
[29] T. Wakasa *et al.*, Nucl. Instrum. Methods Phys. Res. Sec. A **482**, 79 (2002).
[30] W. P. Tan, J. L. Fisker, J. Górres, M. Couder, and M. Wiescher, Phys. Rev. Lett. **98**, 242503 (2007).

[31] W. P. Tan *et al.*, Phys. Rev. C **79**, 055805 (2009).
[32] W. R. Leo, *Techniques for Nuclear and Particle Physics Experiments* (Springer-Verlag, Berlin, 1994).
[33] *MPD-4*; www.mesytec.com/datasheets/MPD-4.pdf.
[34] C. Iliadis, Nucl. Phys. A **618**, 166 (1997).
[35] K. Setoodehnia *et al.*, Phys. Rev. C **83**, 018803(R) (2011).
[36] P. D. Kunz, DWUCK4 code (unpublished).
[37] P. Mohr, Phys. Rev. C **61**, 045802 (2000).
[38] W. A. Fowler, G. R. Caughlan, and B. A. Zimmerman, Annu. Rev. Astr. Astrophys. **13**, 69 (1975).
[39] C. E. Rolfs and W. S. Rodney, *Cauldrons in the Cosmos* (University of Chicago Press, Chicago, 1998).
[40] C. Iliadis, R. Longland, A. E. Champagne, and A. Coc, Nucl. Phys. A **841**, 251 (2010).
[41] T. Rauscher and F.-K. Thielemann, ADNDT **75**, 1 (2000).
[42] V. Z. Goldberg *et al.*, Phys. Atom. Nucl. **68**, 1079 (2005).
[43] J. Görres *et al.*, Nucl. Phys. A **548**, 414 (1992).
[44] V. Z. Goldberg *et al.*, Phys. Rev. C **69**, 024602 (2004).
[45] H.-P. Trautvetter *et al.*, Nucl. Phys. A **297**, 489 (1978).
[46] B. L. Berman, R. L. van Hemert, and C. D. Bowman, Phys. Rev. Lett. **23**, 386 (1996).
[47] F. Kaeppeler *et al.*, Astrophys. J. **437**, 396 (1994).
[48] T. Rauscher, F.-K. Thielemann, J. Görres, and M. Wiescher, Nucl. Phys. A **675**, 695 (2000).
[49] F.-K. Thielemann *et al.*, Adv. Nucl. Astro. **525**, 1 (1987), http://ie.lbl.gov/astro/friedel.html.
[50] R. H. Cyburt *et al.*, Astrophys. J. Suppl. Ser. **189**, 240 (2010).
[51] A. J. Koning, S. Hilaire, and M. C. Duijvestijn, in *TALYS-1.0, Proceedings of the International Conference on Nuclear Data for Science and Technology, April 22–27, 2007, Nice, France*, edited by O. Bersillon, F. Gunsing, E. Bauge, R. Jacqmin, and S. Leray (EDP Sciences, Les Ulix Cedex, France, 2008), p. 211 www.talys.eu/fileadmin/talys/user/docs/talys1.0.pdf.
[52] A. Palumbo *et al.*, Phys. Rev. C **85**, 035808 (2012).